Solid Earth Discuss., 5, 227–256, 2013
www.solid-earth-discuss.net/5/227/2013/
doi:10.5194/sed-5-227-2013

Solid Earth
Discussions
Open Access

An experimental study of pyroxene crystallization during rapid cooling in a thermal gradient; applications to komatiites and chondrites

S. Bouquain[1], N. T. Arndt[1], F. Faure[2], and G. Libourel[2]

[1]LGCA, CNRS UMR 5025, Université J. Fourier, BP53, 38041 Grenoble Cedex, France
[2]Nancy Université, CNRS/INSU, CRPG, 15 rue Notre Dame des Pauvres, 54501Vandoeuvre-les-Nancy, France

Received: 30 November 2012 – Accepted: 8 December 2012 – Published: 27 March 2013

Correspondence to: S. Bouquain (sebastien.bouquain@ujf-grenoble.fr)

Published by Copernicus Publications on behalf of the European Geosciences Union.

Abstract

To investigate the crystallization of pyroxene in spinifex-textured komatiites and in chondrites we undertook a series of experiments in which compositions in the CMAS system were cooling rapidly in a thermal gradient. Cooling rates were generally between 5 to 10 °C h^{-1} but some runs were made at 100–200 °C h^{-1}; thermal gradients were between 10 and 20 °C cm^{-1}. These conditions reproduced those at various levels in the crust of komatiitic lava flow. The starting composition was chosen to have pigeonite on the liquidus and a majority of the experiments crystallized zoned pigeonite-diopside crystals like those in komatiite lavas. A conspicuous aspect of the experimental results was their lack of reproduceability. Some experiments crystallized forsterite whereas others that were run under similar conditions crystallized two pyroxenes and no forsterite; some experiments were totally glassy but others totally crystallized to pyroxene. The degree of supercooling at the onset of pyroxene crystallization was variable, from less than 25 °C to more than 110 °C. We attribute these results to the difficulty of nucleation of pyroxene. In some cases forsterite crystallized metastably and modified the liquid composition to inhibit pyroxene crystallization; in others no nucleation took place until a large degree of supercooling was achieved, then pyroxene crystallized rapidly. Pigeonite crystallized under a wide range of conditions, at cooling rates from 3 to 100 °C h^{-1}. The notion that this mineral only forms at low cooling rates is not correct.

1 Introduction

Pyroxenes in spinifex-textured komatiites and in chondrules display unusual textures and compositional variations that are probably related to the unusual conditions in which they crystallized. In the internal zones of spinifex layers in thick komatiitic basaltic flows, two pyroxenes commonly are present. Where best developed, pyroxene spinifex texture consists of zoned needles with pigeonite cores and augite margins, commonly

organized in clusters that are oriented approximately perpendicular to the flow contacts. Analysis of the compositions of these pyroxenes and of the rocks in which are found has revealed some puzzling features. In many samples pyroxene, usually pigeonite, can be inferred to be the liquidus phase on the basis of textural data, yet when the phase relations of compositions like those of the samples are investigated, it is found that only olivine should have crystallized under equilibrium conditions. The problem has been addressed from a mineralogical and chemical point of view in a companion paper (Bouquain et al., 2009). Here we present the results of a parallel experimental study.

Faure et al. (2006) conducted a series of experiments in which they investigated the origin of spinifex textures. They addressed what has been called the spinifex paradox: the skeletal or dendritic habits of olivine crystals in spinifex textures resemble those in experimental charges that crystallized at high cooling rates (50–100 °C h^{-1}), but these textures are found deep in the interior of lava flows at depths where the cooling rate, limited by conduction through the flow top, must have been low (< 1 to 5 °C h^{-1}). A novel aspect of Faure et al.'s experiments is that they were conducted within the thermal gradient in the upper part of the 1-atm furnace, reproducing the gradient that exists in the upper parts of a lava flow. These experiments produced textures that closely resembled those in olivine spinifex-textured komatiites.

In this paper we present the results of experiments that build on Faure et al.'s work. The major difference is in the composition of the experimental charges: whereas Faure et al. worked on an analogue in the CMAS system of the ultramafic composition of komatiites, we worked on a less magnesian composition, one chosen so that pigeonite was the liquidus phase. With this choice we developed an experimental program designed to help understand the phase relations and habits of pyroxenes that crystallized under conditions like those in komatiitic lava flows and in chondrites.

2 Experimental procedures

The experiments described in this paper were conducted in the experimental petrology laboratory of Centre de Recherches Pétrogaphiques et Géochimiques in Nancy using the method developed by Faure et al. (2006). The starting composition in the CMAS (CaO-MgO-Al_2O_3-SiO_2) system was chosen so as to have pigeonite the liquidus and thus to be comparable to the komatiitic liquids that crystallize pyroxene spinifex textures. The starting material was prepared from pure oxides which were fused in platinum crucibles for 8 h at 1550 °C, a temperature well above the liquidus. The quenched material was then ground to a fine powder in an agate mortar.

For the isothermal crystallization experiments, the powder was mixed with a small amount of polyvinyl alcohol to produce a charge that could be suspended on a platinum wire (Donaldson et al., 1975). The charge was held at constant temperature for several hours in a 1-atm vertical quenching furnace, and quenched in water at the end of the experiment.

For the dynamic crystallization experiments, the powder was packed tightly into a graphite tube (length 5.5–6.5 cm, diameter 4mm) that was placed in a GERO HTRV 70–250 vertical quenching furnace. Depending on the location of the tube above the hot spot of the furnace, the temperature gradient across the experimental charge varied from 8 to 40 °C cm^{-1}. The temperature inside the furnace was measured by PtRh6-PtRh30 thermocouples that had been calibrated by melting gold and palladium wires. Throughout the course of the experiment, a stream of argon maintained a reducing atmosphere, preventing the oxidation of the graphite tubes. In the standard procedure, called procedure 1 (Fig. 1), each experiment began with a stage at which the entire charge was held for one to five hours at a temperature of 1413 °C (1505 °C at the bottom of the charge), about 27–119 °C above the equilibrium liquidus temperature (see Table 1). During this phase, air trapped in the powder escaped, and as the charge compacted during melting, its length decreased from 5–6 cm to 2.5–4.5 cm. The charge was then cooled at a constant rate which varied from 3, 5, 10, 100 to

200 °C h^{-1} depending on the experiment. The temperature gradients across the experimental charge are around 20 °C cm^{-1} and match those calculated in the upper part of a komatiitic flow.

The intent of this procedure was to progressively crystallize the charge, downwards from the cooler top to the warmer base, thus simulating progressive solidification in the upper crust of a lava flow. As described by Faure et al. (2006), this procedure provides important information about the kinetics of crystallization under conditions that reproduce those in natural lavas.

During the experiments labelled CPX15–26, a modified procedure, called procedure 2 (Fig. 1), was used: the experimental charges were first heated to a higher temperature of 1470 °C (1555 °C at the bottom of the charge), 84–169 °C above the liquidus, for two hours, then the temperature was rapidly lowered to bring the top of the capsule (the cool end) to a temperature about 12 °C above the liquidus for one hour. The period of high-temperature fusion resulted in optimal homogenization of the charge and the elimination of any relict solid phases. In the other experiments (those labelled CPX04; CPX06-14), the charges were held at a constant temperature 119 °C above the liquidus for one or several hours. We also performed two experiments with two other similar procedures (procedures 3 and 4, Fig. 1), in order to undoubtedly crystallize pyroxene. In procedure 3, the experimental charge was first heated to a high temperature (1525 °C at the bottom of the charge) for one hour, then the temperature was rapidly lowered to bring the bottom of the capsule to a temperature about that of the liquidus. The charge was then cooled at a constant rate of 3 °C h^{-1}. In the procedure 4, the first heat temperature was very low: 1401 °C at the bottom of the charge, at the hot end. The temperature before the cooling step was also very low: 1325 °C at the bottom of the charge.

At the end of each experiment, the charge was quenched in distilled water. The tube and its experimental charge were then cut along the long axis, imbedded of resin, polished, and then analyzed using an electron microprobe (Cameca SX100 at the University Henri Poincaré, Nancy) and a microfluorescence spectrometer (Eagle III

at the University of Grenoble). An attempt was made to terminate each experiment at a temperature calculated to quench to glass an interval of uncrystallized liquid in the lower (hotter) end of the charge: in practice this proved to be very difficult, as described in the following section.

Figure 2 illustrates a typical experimental charge. The lower third consists mostly of translucent glass which became fractured during quenching. Elongate crystals of pyroxene become increasingly abundant toward the top of the charge and the upper portion is totally crystallized to pigeonite, augite and a silica phase, probably tridymite. The temperatures of initial crystallization of each of these phases can be determined with precision by measuring the position in charge, which was previously calibrated for temperature (Faure et al., 2006). During the experiment CPX15 (Fig. 2), a bubble formed at the bottom of the load because of incomplete outgassing of powder during the initial phase of high-temperature fusion. This happened during several experiments, but does not significantly affect their interpretation (this problem was not encountered during the experiments of Faure et al. (2006) who worked on a less viscous komatiitic composition). In the case of CPX15, the experience was not terminated soon enough to preserve crystal-free glass below the crystallization front. The temperature of the first appearance of pigeonite is therefore a minimum temperature and the estimated degree of nominal undercooling is a maximum value.

The results of the isothermal crystallization experiments are summarized in Table 1 and those of the dynamic cooling experiments are given in Table 2.

2.1 Experimental problems

Many experiments did not work as intended, with variable consequences.

1. The early experiments were carried out in thin graphite tubes that partially disintegrated in the course of the run. In some cases multiple fine, delicate forsterite crystals penetrated the walls of the capsule and grew outwards to form remarkable porcupine-like structures. Although no detailed information about the

crystallization sequence is provided by such experiments, they indicate that forsterite nucleated and grew rapidly at relatively high temperatures, as in the case of experiment CPX06 in which forsterite grew in part of the tube that was at a temperature of 1406 °C at the time of quenching.

2. In several experiments, empty segments of varying size (5–30 mm long) were distributed throughout in the capsule, most commonly near the base or in the middle. We interpret these empty segments as air bubbles that were trapped in the liquid phase during initial melting at high temperatures. Because of the small size of the capsules and the relatively high viscosity of the molten starting material, air trapped in the powder could not always be evacuated. When the air bubble is located at the bottom of the capsule, it has little effect on the course of the experiment. In some experiments, small volumes of melt (a few cubic millimeters) were isolated at the bottom of the capsule, or at the top. The products of crystallization of these melts can be very different from those in the main volume of melt. For example, we observed anorthite and spinel in experiment CPX11, and very Ca-rich diopside in experiment CPX07.

3. It was very difficult to stop the experiments before the crystallization front had reached the base of the capsule. Some experiments were almost entirely glassy or contained only isolated forsterite crystals, and two notable exceptions contained crystal-free glass in the lower portion, but most were entirely crystallized. As discussed below, we infer that the once pyroxene nucleates, it grows rapidly to fill most, or all, of the capsule.

4. The experiments were not reproduceable. The phases that crystallized, and the order in which they appeared, was not systematic but varied from one experiment to another, even when the experimental conditions were similar or identical. For example, experiments CPX14 and CPX15 were conducted at identical cooling rates (10 °C h^{-1}) and in the same thermal gradient (20 °C cm^{-1}). The temperatures at capsule ends at the time of quenching were similar: 1336 °C and 1352 °C at

the hot end and 1272 °C and 1278 °C at the cool end. Yet despite these similar conditions, forsterite is present in experiment CPX14 (as isolated hopper crystals) but is absent in experiment CPX15. In addition, the morphologies of pyroxene are very different in the two experiments, as described in the section presenting the results of the dynamic cooling experiments.

3 Experimental results

3.1 Isothermal crystallization experiments

The isothermal crystallization experiments were employed to determine the liquidus phase relations of the starting material. The material used in the dynamic cooling experiments (Table 1) was chosen to have pigeonite in the liquidus and appropriately only this mineral crystallized in experiment SB613, which was conducted at 1385 °C. The crystals are rounded, with sizes ranging from 5 to 30 µm. The calcium content of this pigeonite is very low, around 3.1 wt% CaO. The nucleation was heterogeneous and took place on the platinum wire, on the walls of the charge, on a platinum bead that became detached during the preparation of the experiment, and on an air bubble. In an experiment conducted at 1388 °C, the entire charge (SB623) is glassy. The temperature liquidus is therefore 1386 ± 1 °C. Only pigeonite crystallizes at temperatures down to 1359 °C, and its Ca content increases gradually from 3.1 % to 6.0 wt% (SB625). At 1354 °C, diopside appears as abundant, rounded, very small crystals, each a few microns across. The rate of nucleation of diopside was evidently higher than that of pigeonite. A silica mineral, probably tridymite, joined the assemblage to 1348 °C (SB618). When it first appears, this mineral has an elongate anhedral habit but at lower temperature it forms euhedral laths that are highly elongated along the c axis. The solidus temperature was not determined because there was still a fraction of the liquid at 1277 °C (SB630).

We also performed six other series of isothermal crystallization experiments, each with a different starting material composition (Fig. 3). The results are shown in Fig. 4. This phase diagram represents the 5 % An plane in the forsterite-diopside-anorthite-silica system, which is part of the CMAS system. The size of the pigeonite field decreases with increasing anorthite component and disappears completely at moderate Al_2O_3 contents (Longhi and Boudreau 1980).

3.2 Dynamic crystallization experiments

Major results of dynamic crystallization experiments are summarized in Fig. 7. Associated data are in Table 2. Nomenclature is from Donaldson (1976) and Faure et al. (2003).

Forsterite: in many of the dynamic crystallization experiments, we observed forsterite in addition to one or two pyroxenes. Forsterite crystallized in approximately one third of the experiments, an unexpected result because this mineral did not crystallize in any of isothermal crystallization experiments. In some experiments it coexists with tridymite and is evidently not an equilibrium phase in the starting material. Forsterite was the only crystalline phase in four experimental runs (Table 2), all conducted at a moderate cooling rate of 5 °C h^{-1}. In experiments with higher cooling rates (100–200 °C h^{-1}) forsterite did not appear. In most experiments, the forsterite crystals have euhedral, or elongate platy, or dendritic habits (Fig. 5). In the runs labelled CPX03 and CPX04, conducted with a low thermal gradient (10 °C cm^{-1}), a few euhedral forsterite crystals with well-developed faces were observed at the base of the capsule (Fig. 5f). These experiments were quenched at about 1380 °C. The crystals contain about 0.7 wt % CaO, and residual glass has a forsterite-depleted composition, with lower SiO_2 and higher CaO, compared to the starting material.

In the two other experiments (CPX02 and CPX06), forsterite displays dendritic morphologies. The CPX02 experimental charge contains two parts: the 12 mm-long lower part contains mm-sized elongate platy crystals with fine dendrite tips (Fig. 5b), and the 10 mm-long upper part displays fine dendritic crystals (Fig. 5a). The latter nucleated

on the capsule border, and are 100–300 µm long. The residual glass is strongly zoned around the forsterite crystals. CPX06 was not a successful run because the graphite capsule partially disintegrated but in this experiment olivine grew at a very high temperature (1406 °C).

In experiments in which olivine coexists with pyroxene, the forsterite habit is generally similar to that in pyroxene-free runs, but in some case the borders of the crystals are rounded and embayed. Experiment CPX09 (Fig. 8) contains good examples of the variety of textures deployed by this mineral. In the lower part of the capsule, forsterite has a hopper or platy habit (Fig. 6c) whereas at the top of the capsule, it forms crystals with a complex, irregular, elongate morphology. Pigeonite and diopside grow around forsterite crystals (Fig. 6a, b). Some of the forsterite crystals are rounded and embayed, particularly where they are surrounded by smaller pigeonite and diopside crystals (Fig. 6a, b).

The forsterite crystals have high CaO contents, up to 0.5 % in solid crystals and more in fine dendrites. We were not able to measure CaO contents in fine dendrites because of their extreme thinness, but BSE images (Fig. 5e) show enrichment in this heavy component in dendrites. The glass immediately surrounding the fine dendrites is strongly depleted in the forsterite component, with low SiO_2 and high CaO compared to starting material. A strong chemical gradient is present around dendritic crystals.

Pyroxene crystallized over a large range of temperatures, from 1365 °C to 1102 °C. In these experiments, cooling rates were between 3 and 100 °h^{-1} and the temperature gradient was 20 °C cm^{-1}. One or two pyroxenes, pigeonite and diopside, crystallized in about two thirds of the experiments. The two pyroxenes coexist in all experiments except for CPX08, the unsuccessful experiment with porcupine-like forsterite, where only diopside crystallized. Pigeonite and diopside were present over the entire temperature range but diopside appears in only one experiment at a temperature over 1336 °C. Isolated crystals of pigeonite were observed in only one run, CPX 15; in all others this mineral occurs as the cores of zoned crystals with diopside margins.

Pyroxene usually crystallizes as acicular, zoned crystals, each with a core of pigeonite and a border of augite (e.g. Figure 6e, f). In experiment CPX09, the larger zoned crystals have a "plumose" morphology (Fig. 6c) while the smaller diopside crystals have a more euhedral, prismatic or chain-like morphology (Fig. 6b). In other experiments such as CPX19 and CPX22, pyroxene forms complex or cross-shaped dendrites (Fig. 6d). In the two experiments conducted under similar conditions but with contrasting results, the pyroxene morphologies were very different. As mentioned above, forsterite crystallized as isolated hopper crystals in experiment CPX14, but was absent in experiment CPX15. In experiment CPX14, skeletal prismatic to highly dendritic grains of pyroxene crystallized between larger forsterite grains, like those illustrated in Fig. 6b, c. In experiment CPX15, pyroxene crystals fill the entire charge, mainly as elongated needles oriented parallel to one another and approximately parallel to the walls of the capsule. As illustrated in Fig. 2, in the lower, hotter, part of the capsule, pigeonite occurs alone as acicular, dendritic crystals; in the upper, cooler part, diopside and pigeonite crystallized as a dense mat of fine, zoned, dendritic crystals. In the uppermost part, tridymite appears in the matrix (Fig. 2).

In experiment CPX22, pigeonite and diopside crystallize as zoned cross-shaped dendrites. These are found in the lower part of the capsule, at a temperature of 1365 °C, 9 °C above diopside liquidus temperature as determined in isothermal experiments.

Representative pyroxene compositions are given in Table 3. The CaO content of pigeonite varies from 3.9 % in the core of a grain that crystallized at the highest temperature, to an apparent 9 % in a grain in one of the lowest-temperature runs. The high value could be a bad analysis resulting from a mixed signal between the pigeonite core and the diopside border of a fine zoned crystal.

Most diopside grains have CaO contents between 13 % and 20 %. In the run CPX08, where diopside formed complex dendritic crystals, the cores are unusually calcic (25 %) and the borders are rich in Al (2 %).

Other minerals. Silica phase (probably tridymite) is present in about one-third of experimental charges, irrespective of the presence of forsterite. Other crystalline phases

include Ca-rich pyroxene (CPX07), anorthite (CPX11) and spinel (CPX11). In all three cases, these minerals crystallized in small volumes of liquid, commonly isolated from the main mass of the charge and they are not representative of the normal crystallization sequence.

4 Discussion

Perhaps the most significant aspect of the results is their unpredictability. Although other experiments have explored the crystallization of Ca-poor pyroxene under conditions of rapid cooling (Kinzler and Grove, 1985; Parman et al., 1997), none has coupled this with the presence of a thermal gradient. Under such conditions the kinetics of nucleation and crystallization come into play and strongly influence the sequence and extent of crystallization, or, under some circumstances, the very presence or absence of certain phases.

4.1 Olivine presence problem

Forsterite, a phase absent under equilibrium conditions, crystallized in a third of our experiments. It is present in one run (CPX 06) at a temperature of 1406 °C but absent from another run (CPX10) that was quenched at far lower temperatures, from 1307 to 1269 °C. In the latter, the entire charge was glassy and no crystalline phases are present. Another example is the contrasting phase assemblages of experiment CPX14, which crystallized forsterite, and CPX15, which did not, as discussed in the preceding section. Finally, diopside is present at the bottom of the capsule CPX22, at a temperature of 1365 °C, 9 °C above its liquidus temperature. This apparently high value, could be due to a sedimentation problem of big crystals during experiment. Crystallization of forsterite and pigeonite may have produced an evolved liquid from which diopside then crystallized. Temperature of crystallization of diopside from this liquid may be slightly different from diopside equilibrium liquidus temperature.

Another interesting element is the difficulty we experienced in quenching the runs before they had entirely crystallized. In the earlier experiments carried out by Faure et al. (2006) on charges of more magnesian compositions, it was relatively simple to terminate the experiment at a stage when a totally glassy segment was preserved in the lower, hotter, portion of the capsule, but in our experiments, either the charge was totally glassy (e.g. CPX 10) or crystals were present throughout the charge.

The explanation of these results probably can be found in the kinetic effect and particularly in the difficulty of nucleation of pyroxene. Kinzler and Grove (1985) and Parman et al. (1997) have shown, for example, that under conditions of rapid cooling (but in the absence of a thermal gradient), the temperature of appearance of augite and pigeonite was suppressed when the cooling rate exceeded 10 °C h^{-1}. Kinzler and Grove found that at a cooling rate of 50 °C h^{-1}, the nucleation of augite was delayed by 100 °C and that of pigeonite by 250 °C. Faure et al. (2006) observed a similar effect in the presence of a thermal gradient. In experiments conducted at a cooling rate of 5 °C h^{-1}, the diopside liquidus was suppressed by about 46 °C. A significant difference is that whereas the suppression of the forsterite liquidus was very small in the normal dynamic crystallization experiments, Faure et al. monitored a ∼ 50° suppression in the thermal-gradient experiments.

In our experiments we observed a somewhat contrary effect: as summarized in Figs. 7 and 9, forsterite appears in our dynamic-cooling thermal-gradient experiments as an apparently metastable phase at temperatures above the liquidus measured in the equilibrium experiments. Even if the presence of porcupine-like olivine in flawed experiment CPX06 is discounted, the crystals in experiment CPX04 cannot be so easily dismissed. In the latter experiment, the olivine has the euhedral morphology illustrated in Fig. 5f and is found at the base of the capsule. It is possible that these crystals nucleated in the upper, cooler portion of the capsule, but since the thermal gradient was low, the temperature even at this end was high, at 1356 °C. At the hotter base of the capsule where the euhedral crystals were found, the temperature at the time of quenching was 1385 °C, essentially the same as the 1386 °C liquidus under equilibrium conditions.

In experiment CPX09, shown in Fig. 8, olivine persists from the base to the top of the capsule. At the hot base (temperature at quenching = 1298 °C), it forms the stubby to moderately elongate crystals shown in Fig. 5c, d; in the middle it occurs as finer, more elongate plates; and at the top (temperature at quenching = 1230 °C) it occurs as large plates with smoothly curved or embayed margins, as shown in Fig. 5a, b. The olivine crystals appear to have grown on the borders of the capsules and on small particles of platinum, and apparently nucleated heterogeneously. Several lines of evidence indicate that the forsterite is metastable: first and most obviously, its absence in the isothermal experience conducted on the same starting material; second, its coexistence with silica phase (tridymite) in one experiment (CPX25); third, the curved and embayed margins of the grains at the top of capsule CPX09, which we interpret to indicate that the crystals were reacting with the liquid.

The presence or absence of olivine is influenced, though not totally controlled, by the experimental procedure. Olivine is present in all crystallized experiments that were initiated by heating at temperatures only moderately higher than the liquidus (1505 °C – procedure 1) and is absent in all but two of the experiments that were initiated by heating at the higher temperature of 1555 °C (procedure 2). In both experiments that were initiated by heating at low and moderate temperatures and then rapidly cooled to temperatures below the liquidus in the entire charge (procedures 3 and 4, see Fig. 1), olivine is absent.

4.2 Crystallization of pigeonite and zoned pyroxene crystals with various morphologies

The capacity of pyroxene to grow rapidly once it nucleated is illustrated in the image of the experimental charge CPX15 in Fig. 2. Pyroxene fills the whole capsule, from the cool top, which was quenched at 1278 °C, to the hot base quenched at 1352 °C. In this charge pyroxene crystallized at temperatures far higher than those in experiment CPX10, which was entirely glassy even though it was quenched at a lower temperatures of 1269 to 1307 °C. Pyroxene is absent at the hot end (1298 °C) in experiment

CPX09, where only olivine has crystallized. The differences in the phase assemblages can in part be attributed to the experimental conditions. The cooling rate in experiment CPX10, which produced as entirely glassy charge, was 200 °C h^{-1} and this rapid rate no doubt prevented nucleation. For experiment CPX15, in which the charge shows long acicular crystals of pyroxene, procedure 2 was used and it is possible that the initial period of high-temperature heating destroyed the relict structures in the liquid that in other experiments facilitated the nucleation of olivine, as discussed by Lofgren (1983). It appears that during experiment CPX15 no olivine crystallized at high temperatures and once pyroxene nucleated it grew rapidly to fill the entire capsule. In experiment CPX09, conducted using procedure 1, pyroxene also nucleated and it crystallized throughout the upper two-thirds of the capsule. However, in this case it did not penetrate into the lower portion of the capsule, presumably because the composition of the liquid had been modified by the growth of the large olivine crystals.

Another aspect that needs to be emphasized is the presence of pigeonite even in rapidly cooled runs. Zoned crystals with pigeonite cores are present in experiments CPX19 and 26, both of which were cooled at 100 °C h^{-1}. The idea that pigeonite only forms at slow cooling rates less than 10 °C h^{-1} (Kinzler and Grove, 1985; Parman et al., 1997) is clearly not valid.

4.3 Application to natural rocks

One important goal of our study was to understand the conditions in which pyroxene crystallizes in komatiites. Although this goal has been realized in a broad sense, several important differences between the environment of crystallization in the interior of a komatiite flow and our experimental setting limit the application of our results. Our experiments have demonstrated how subtle differences in pre- or syn-crystallization conditions can significantly change the order of crystallization and the compositions of the phases that crystallize. In the interiors of komatiite lava flows conditions were far less extreme than those in our experiments. For example, although it can be argued that some komatiites became superheated during their passage from mantle source to

the surface (REFS), most komatiites contained olivine phenocrysts when they erupted which indicates that on eruption they were effectively at their liquidus. Furthermore, in the interior of a lava flow, at tens to hundreds of centimetres beneath the flow top, cooling rates are limited by conduction through the solid crust of the flow – and eventually convection in large komatiite flows – and are relatively low. At the depths of several metres below the flow top, the level at which pyroxene spinifex texture forms, cooling rates were below 1 °C h^{-1} (Turner et al., 1986). The fact that we grew zoned pyroxene crystals with pigeonite cores and diopside mantles in our experiments is significant because the similarity between these crystals and those in natural komatiites indicates that we have reproduced the essential features of the natural environment. In both settings the pyroxene grains crystallize during constrained growth in a thermal gradient. The growth starts at the cool end of the experimental charge or lava flow, then proceeds downwards. However, many specific aspects of the experimental results, such as the appearance of metastable olivine, have no direct application to komatiite crystallization. In almost all natural lava flows the liquidus mineral is olivine and pyroxene spinifex forms in evolved liquids developed by extraction of olivine, usually into the cumulate base of the lava flow. Under conditions of slower cooling in systems in which olivine has crystallized in the lower part of the unit, this mineral will not grow metastably.

An area where our results may have direct application is in the interpretation of textures in chondrites, where olivine and pyroxene with skeletal and dendritic habits are found (Lofgren and Lanier, 1990; Lofgren and Russell, 1986; Lofgren, 1989).

5 Conclusions

- Spinifex textures result from crystallization at moderate cooling rates within a thermal gradient. Analogues of komatiitic basaltic compositions crystallize zoned crystals with pigeonite cores and diopside (or augite) margins.
- Pigeonite formed at cooling rates up to 100 °C h^{-1}.

– Large degrees of undercooling occur at the onset of crystallization of pyroxene crystals (both pigeonite and augite).

– Under conditions of moderate cooling rate, forsterite crystallizes metastably from a liquid with pigeonite at the liquidus. If the liquid if heated to high temperatures before rapid cooling, pyroxene nucleation is strongly delayed but once crystallization starts it proceeds rapidly.

References

Bouquain, S., Arndt, N. T., Hellebrand, E., and Faure, F.: Crystallochemistry and origin of pyroxenes in komatiites and lunar basalts, Contrib. Mineral. Petrol., submitted, 2009.

Donaldson, C. H.: An experimental study of olivine morphology, Contrib. Mineral. Petrol., 57, 187–213, 1976.

Donaldson, C. H., Williams, R. J., and Lofgren, G.: A sample holding technique for study of crystal growth in silicate melts, Am. Mineral., 60, 324–326, 1975.

Faure, F., Trolliard, G., Nicollet, C., and Montel, J.-M.: A developmental model of olivine morphology as a function of the cooling rate and the degree of undercooling, Contrib. Mineral. Petrol., 145, 251–263, 2003.

Faure, F., Arndt, N. T., and Libourel, G.: Formation of spinifex texture in komatiites: an experimental study, J. Petrology, 47, 1591–1610, 2006.

Kinzler, R. J. and Grove, T. L.: Crystallization and differentiation of Archean komatiite lavas from northeast Ontario: phase equilibrium and kinetic studies, Am. Mineral., 70, 40–51, 1985.

Lofgren, G. E.: Effect of heterogeneous nucleation on basaltic textures: a dynamic crystallization study, J. Petrol., 24, 229–255, 1983.

Lofgren, G. E.: Dynamic cyrstallization of chondrule melts of porphyritic olivine composition: textures experimental and natural, Geochim. Cosmochim. Ac., 53, 461–470, 1989.

Lofgren, G. and Lanier, A. B.: Dynamic crystallization study of barred olivine chondrules, Geochim. Cosmochim. Ac., 54, 3537–3551, 1990.

Lofgren, G. and Russell, W. J.: Dynamic crystallization of chondrule melts of porphyritic and radial pyroxene composition, Geochim. Cosmochim. Ac., 50, 1715–1726, 1986.

Longhi, J. and Boudreau, A. E.: The orthoenstatite liquidus field in the system forsterite-diopside-slica at one atmosphere, Am. Mineral., 65, 563–573, 1980.

Parman, S., Dann, J., Grove, T. L., and de Wit, M. J.: Emplacement conditions of komatiite magmas from the 3.49 Ga Komati Formation, Barberton Greenstone Belt, South Africa, Earth Planet. Sci. Lett., 150, 303–323, 1997.

Turner, J. S., Huppert, H. E., and Sparks, R. S. J: Komatiites II: experimental and theoretical investigations of post-emplacement cooling and crystallization, J. Petrol., 27, 397–437, 1986.

Table 1. Isothermal crystallization experiments with composition A.

# Run	T (°C)	Melting time (h)	Fe-free pigeonite	Ca-rich diopside	Silica
SB632	1320	102	+	+	+
SB633	1340	24	+	+	+
SB618	1348	100	+	+	+
SB626	1354	15	+	+	–
SB625	1359	7	+	–	–
SB627	1364	7.5	+	–	–
SB615	1379	15.3	+	–	–
SB613	1385	11.2	+	–	–
SB623	1388	9	–	–	–
SB624	1389	14.7	–	–	–
SB622	1394	96	–	–	–
SB611	1486	1.3	–	–	–

Notes:
+ = present.
– = absent.

Table 2. Dynamic crystallization experiments data.

# Run	Cooling rate (°C h^{-1})	Thermal gradient (°C cm^{-1})	Starting temperature* (°C)	T_{quench}° (°C)	Total run duration (h)	Degree of superheating° (°C)	# Procedure	Forsterite	Pigeonite	Diopside	Other minerals	Special
CPXI 01	5	22.7	1401	1247/1118	18.7	15/-94	3	–	a	a	silica	
CPXI 02	5	13.7	1488	–	?	102/70	1	p, ld	–	–	–	stopped before the end
CPXI 04	5	10.7	1478	1385/1356	20	92/64	1	e	–	–	–	
CPXI 05	3	21.7	1525	1188/1102	67.5	139/60	4	–	a	a	silica	
CPXI 06	5	16.8	1505	1406/1389	21.5	119/103	1	ld	–	–	–	"porcupine-like" forsterite
CPXI 09	10	21.6	1505	1298/1230	24.5	119/47	1	h, p	plu, ch	plu, ld	–	
CPXI 10	200	18.7	1505	1307/1269	2	119/83	1	–	–	–	–	glass only
CPXI 14	10	20	1505	1336/1272	20	119/57	1	h	c	c	–	
CPXI 15	10	20.7	1505	1352/1278	20	119/34	2	–	a	a	silica	
CPXI 19	100	18.5	1505	1361/1320	4.5	119/79	2	–	plu, cd	plu, cd	–	
CPXI 22	10	20	1505	1365/1307	17.1	119/64	2	h	c	c	–	
CPXI 26	100	21.0	1505	1317/1224	4.8	119/31	2	–	a	a	silica	

Notes:
* at the bottom of the charge.
° at the bottom/at the top of the charge.
– = absent.
e = euhedral.
h = hopper.
a = acicular.
p = platy olivine.
ch = chain-like.
ld = linear dendrites.
cd = crossed dendrites.
plu = plumose.
c = complex crystals.

Table 3. Liquid and mineral compositions.

	Starting material (composition #8)	Isothermal crystallization experiments #SB633				Dynamic crystallization experiments#CPX15		
	glass	glass	pigeonite	diopside	silica	glass	pigeonite	diopside
MgO	21.6	16.6	35.8	24.6	0.0	18.1	37.2	28.2
Al_2O_3	1.6	3.6	n.d.	0.1	0.2	2.7	0.1	0.1
SiO_2	62.3	63.8	59.9	57.3	99.4	64.4	60.9	58.3
CaO	14.7	15.4	5.7	18.7	0.1	16.3	3.9	14.9

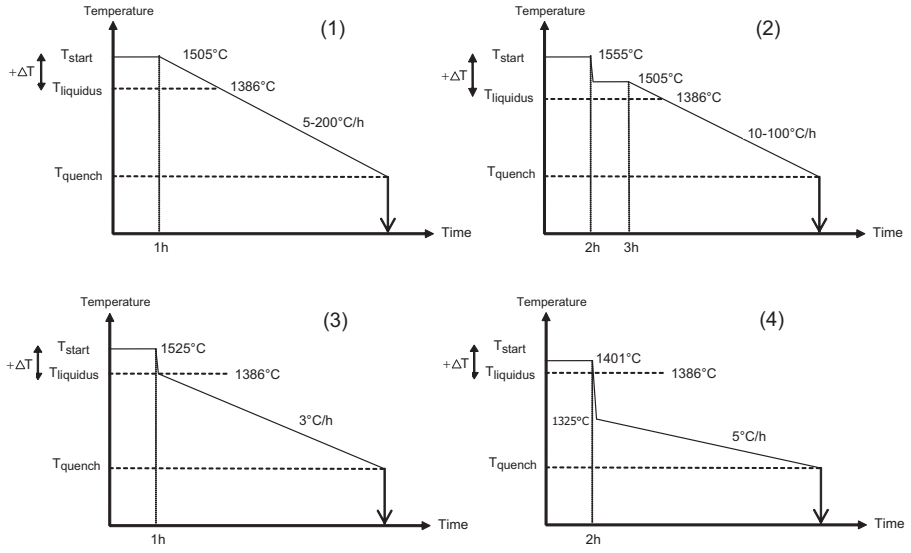

Fig. 1. Details of the four procedures of cooling used during dynamic crystallization experiments.

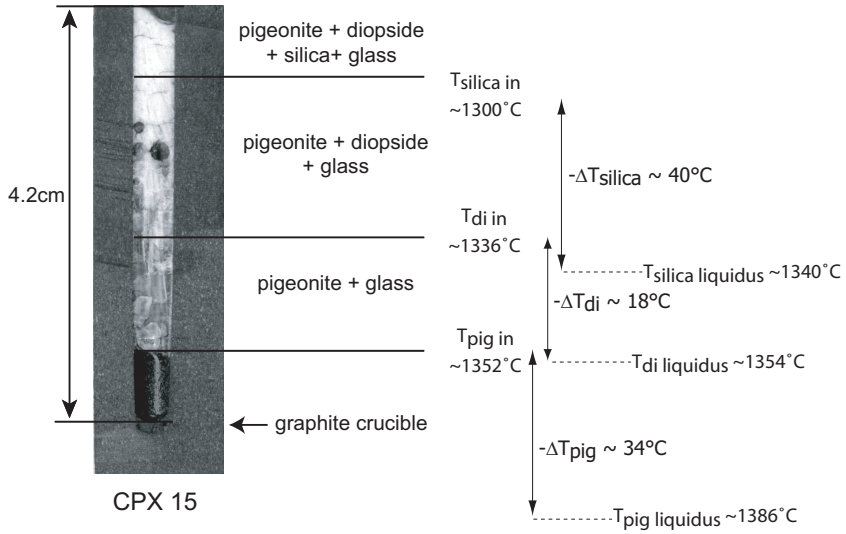

Fig. 2. Typical experimental charge. The charge was cut along its length, then polished and scanned. Temperatures of appearance of crystalline phases are compared to their liquidus temperature determined in isothermal experiments.

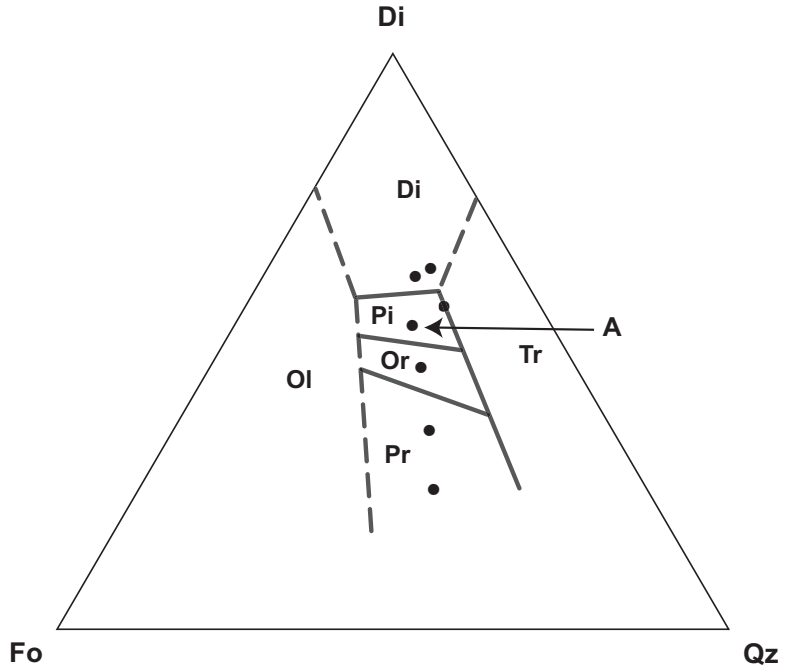

Fig. 3. Starting material compositions plotted in the forsterite (Fo) – diopside (Di) – silica (Qz) pseudo-ternary. Liquid compositions are projected from anorthite. Phase boundaries and reaction curves are also shown from Fig. 4. Composition A was used in dynamic crystallization experiments.

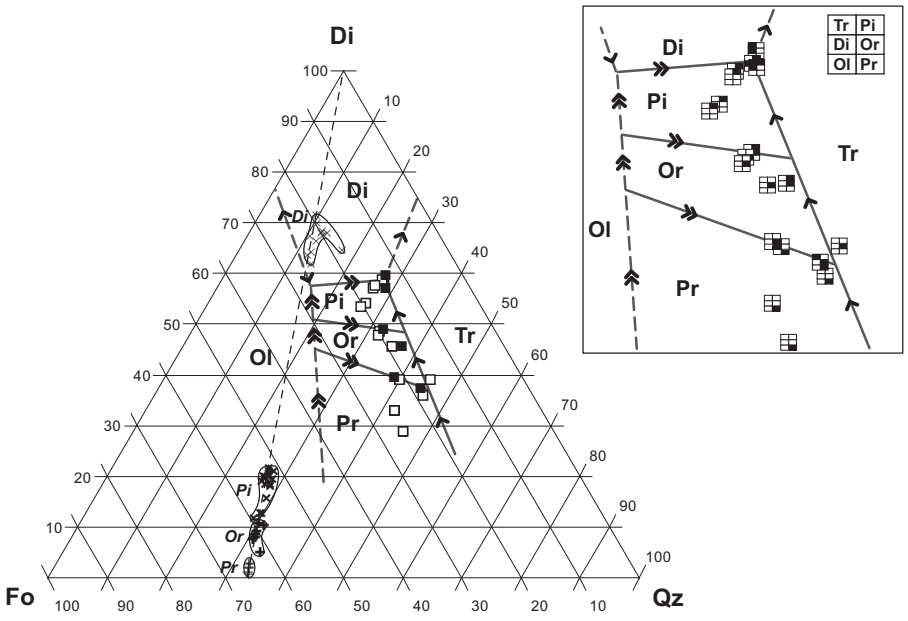

Fig. 4. Liquidus boundaries in the system forsterite-diopside-anorthite-silica. Represented join is $Fo_{95}An_{05}$-$Di_{95}An_{05}$-$SiO_{295}An_{05}$: this plane is parallel to the pseudo-ternary Fo-Di-SiO_2 and contains 5 % An. Squares are liquid compositions saturated with two crystalline phases (white squares) or three crystalline phases (black squares). Analysis of pyroxene crystals are also drawn. Single arrows indicate cotectic curves; double arrows indicate reaction curves.

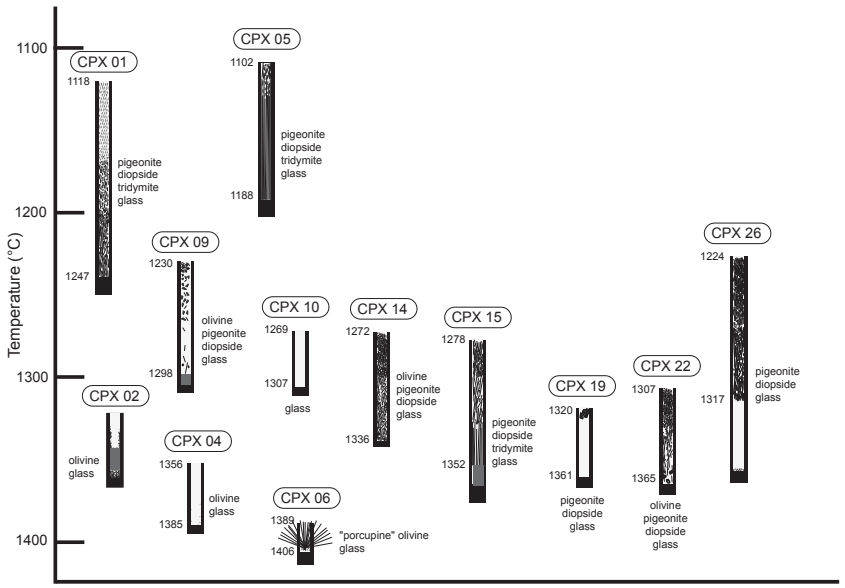

Fig. 5. Textural and mineralogical data from dynamic crystallization experiments. The graphite capsules are represented in black. Minerals are in black and lie in a glass shawn in white. Grey fields are bubbles.

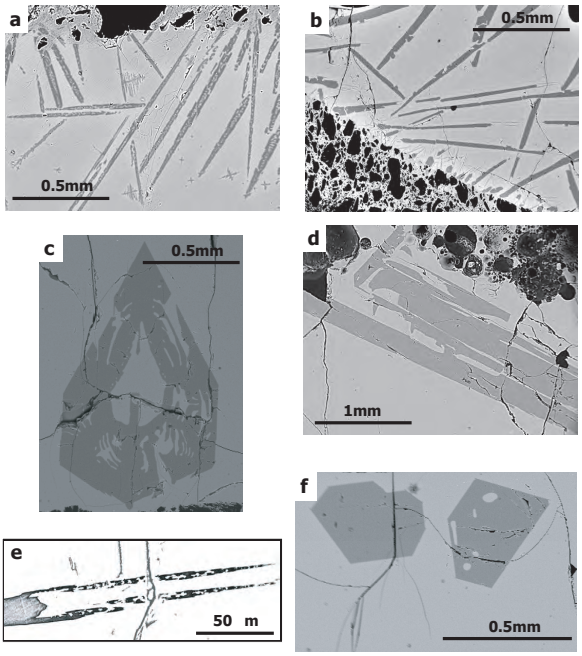

Fig. 6. Photomicrographs showing olivine morphologies observed in dynamic crystallization experiments. Nomenclature is from Donaldson (1976) and Faure et al. (2003), respectively. **(a)** Chain olivine/swallowtail shape (CPX02). **(b)** Branching olivine/swallowtail shape (CPX02). **(c)** Hopper olivine (CPX09). **(d)** Plate olivine/swallowtail shape (CPX09). **(e)** Detail of dendritic tail of a swallowtail olivine crystal (CPX02). **(f)** Polyhedral olivine (CPX04).

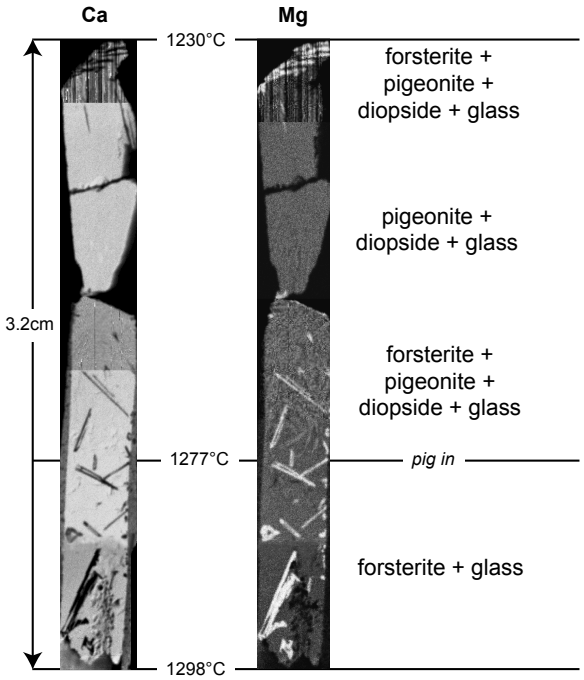

Fig. 7. Microfluorescence images of the experimental charge labelled CPX09. Indicated temperatures are quenched temperature.

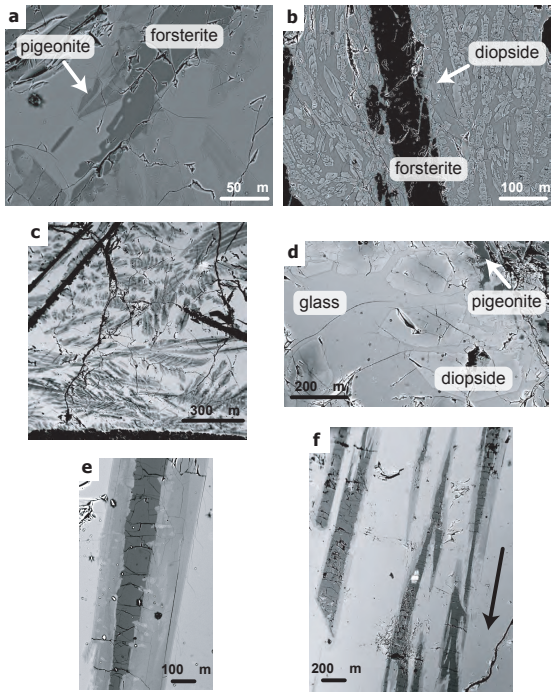

Fig. 8. Photomicrographs showing pyroxene morphologies observed in dynamic crystallization experiments. **(a)** Dendritic pigeonite growing on a rounded forsterite crystal (CPX09). **(b)** Chain diopside nucleation and growth on a plate olivine crystal. **(c)** Plumose zoned pyroxene between platy olivine crystals (CPX09). **(d)** Dendrites on complex pyroxene crystal (CPX14). (**e** and **f**) Zoned pyroxene needles, growing downwards and parallel to each other.

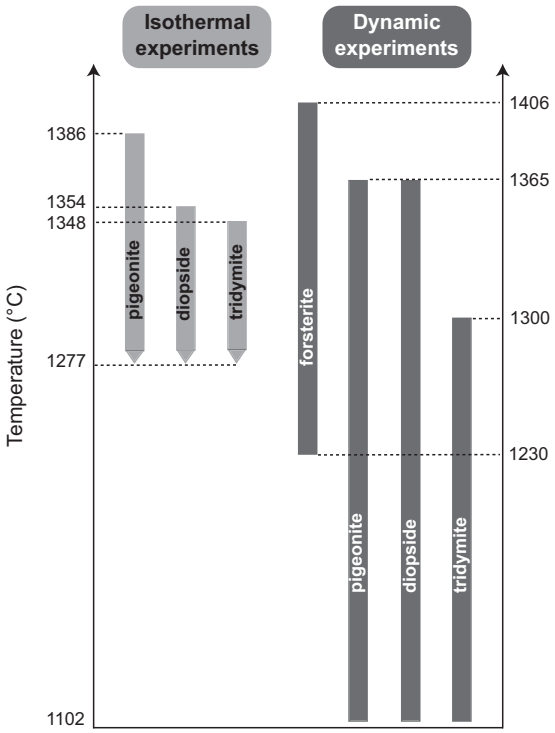

Fig. 9. Range of crystallization temperatures of silicate phases observed in both isothermal and dynamic experiments.